FLOMEKO2019
18th International Flow Measurement Conference
Portugal | Lisbon | LNEC | 26-28 june 2019

Discharge coefficients of CFVN predicted for high Reynolds numbers based on Low-*Re*-calibration

B.Mickan[1]

[1]Physikalisch-Technische Bundesanstalt, Bundesallee 100, D-38116 Braunschweig, Germany
E-mail (corresponding author): bodo.mickan@ptb.de

Abstract

In 2016, PTB introduced a function for the representation of the discharge coefficient c_D of critical flow venturi nozzles (CFVN) (versus the Reynolds number *Re*) what covers the operating range with laminar boundary layers and with turbulent boundary layers as well. It contains the parameters *a* for the impact of the core flow, b_{lam} for the *Re*-dependency in case of laminar and b_{turb} in case of turbulent boundary layers. These parameters are not independent to each other but have the fixed relation of $b_{turb} = 0.003654 b_{lam}^{1.736}$.
Furthermore, the parameter *a* and the parameter b_{lam} are both direct functions of the local curvature radius $R_{c,throat}$ of the nozzle at the throat. These relationships to $R_{c,throat}$ are described by theoretical models. Consequently, the overall dependency of the discharge coefficient c_D on Reynolds number *Re* can be derived from only one parameter.
The paper describes how the relationships mentioned above can be used to extrapolate the calibration values of a CFVN determined with atmospheric air to high pressure gas flow applications covering a Reynolds range of about 1:60. It is shown in detail by examples and the reliability is demonstrated by comparison data for low and high pressure of 33 nozzles. Finally, aspects of preconditions for such extrapolation and uncertainties will be discussed.

1. Introduction

1.1 Motivation and idea

In 2016, a functionality for the discharge coefficient c_D versus Reynolds number were successfully introduced to cover the operating of critical nozzles with laminar as well as turbulent boundary layers using only three parameters [1]. The outcome of this extended analysis of inter comparison data using this functionality as the base for LS-fitting indicated that there were only small differences left to the measured data in the order of 0.1 % and lower. With this, the question raised up if it is possible to use only the data at low Reynolds numbers (e.g. the measurements with air at atmospheric conditions) for such parameter determination and to use the functionality to get a reliable extrapolation to the high Reynolds numbers even to the range above $Re \geq 2 \cdot 10^6$.

The data for atmospheric air usually do not cover a wider range of Reynolds numbers but have to be considered approximately as a single point measurement, therefore it was necessary in a first step to make further effort in the mathematical model to reduce the number of free parameters down to one. Nevertheless, it can be demonstrated here on the data base containing 33 different nozzles that this approach is reasonable.

1.2 Mathematical Model

The discharge coefficient of a sonic nozzle can be described as a combination of two independent displacement effects. At one side we have the effect of the two dimensional core flow $c_{D,TwoDim}$ and on the other side the displacement effect of the boundary layer $c_{D,BoundLayer}$:

$$c_D = c_{D,TwoDim} \cdot c_{D,BoundLayer} \quad (1)$$

The displacement effect of the boundary layer can be described as a reduction of the geometrical cross section area A_{geom} by the complete area covered by the displacement thickness δ_1 of the layer:

$$c_{D,BoundLayer} = \frac{A_{geom} - A_{BoundLayer}}{A_{geom}} = \left(1 - 2\frac{\delta_1}{d}\right)^2 \quad (2)$$

Replacing $c_{D,TwoDim}$ with the parameter a, the discharge coefficient can be expressed as:

$$c_D = a\left(1 - 2\frac{\delta_1}{d}\right)^2 \approx a - \frac{\delta_1}{d} = a - \frac{b}{Re^n} \quad (3)$$

The dependency on Reynolds number Re is different for laminar and turbulent boundary layers, expressed by different values of the exponent n in Equation (3):

$$\begin{aligned} c_{D,lam} &= a - b_{lam} Re^{-0.5} \; for\; laminar\; BL \\ c_{D,turb} &= a - b_{turb} Re^{-0.139} \; for\; turbulent\; BL \end{aligned} \quad (4)$$

For the parameters a and b_{lam}, there are theoretical solutions available, for a e.g. the solution of Kliegel [2] and for b_{lam} the solution of Geropp [3][4]. For both, these theoretical approaches provide the solution in dependency on the curvature radius of the nozzle at the throat $R_{C,throat}$ as a common parameter. So, for the parameter a yield:

$$a = 1 - a_2 + a_3 - a_4 \quad (5)$$

with

$$a_2 = \frac{\kappa+1}{96(2R_{C,throat}+1)^2}$$

$$a_3 = \frac{(\kappa+1)(8\kappa-27)}{2304(2R_{C,throat}+1)^3}$$

$$a_4 = \frac{(\kappa+1)(754\kappa^2-757\kappa+3633)}{276480(2R_{C,throat}+1)^4}$$

And for the parameter b:

$$b_{lam} = G \cdot R_{C,throat}^{0.25} \quad (6)$$

For our purpose to reduce the number of free parameters we use the fact that the theoretical approaches for parameter a and b_{lam} are based both on the curvature radius $R_{C,throat}$ at the throat. The real curvature radius determining these parameters probably differs from $R_{C,throat}$, but we assume that it is for both the same (virtual) curvature Radius $R_{C,virt}$. Finally, only the parameter b_{lam} remains as a free parameter and the other are linked to it via the relationships of Equations (5)(7) and (8)

$$R_{C,virt} = \left(\frac{b_{lam}}{G}\right)^4 \quad (7)$$

$$\begin{aligned} b_{lam} &\underset{(7)}{\rightarrow} R_{C,virt} \underset{(5)}{\rightarrow} a \\ b_{turb} &= 0.003654 b_{lam}^{1.736} \end{aligned} \quad (8)$$

Both, the parameter a [Equation (5)] and the factor G depend on the isentropic exponent κ of the gas. Furthermore, the factor G is a function of the Prandtl number and the wall temperature (rsp. the difference between wall and gas). With this, we have dependencies of the c_D-values not only on Reynolds number but also slightly on the gas properties. Although we already know that the relationship given by Geropp [4] for the factor G in Equation (6) is not totally satisfying (see also[5][6]), we keep this here for our approach in same way as it was discussed in [1].

It is appropriate to bridge the laminar and turbulent boundary layer transition with one function shown by Equation (9) for the whole Reynolds range by means of a transition function given by the two weighing terms s_{lam} and s_{turb}. The parameter Re_{tr} defines the middle point of the transition and k_u the "sharpness" of the transition (the larger k_u, the more "sudden" the transition occurs).

$$\begin{aligned} c_D = {} & s_{lam} \cdot c_{D,lam} + s_{turb} \cdot c_{D,turb} \\ \text{with} \quad & s_{lam} = 0.5\left\{1 - \tanh\left[k_u \log\left(\frac{Re}{Re_{tr}}\right)\right]\right\} \\ & s_{turb} = 1 - s_{lam} \end{aligned} \quad (9)$$

For the investigation here in this paper we fix the values arbitrarily to $k_u = 5.5$ and $Re_{tr} = 1.25 \cdot 10^6$. It is based on all the experience in the past and we will discuss later what conclusion we can derive from this. With these values, the range of transition between laminar and turbulent boundary layers is expected to occur between approximately $Re = 7 \cdot 10^5$ and $Re = 2.5 \cdot 10^6$, see also Figure 1.

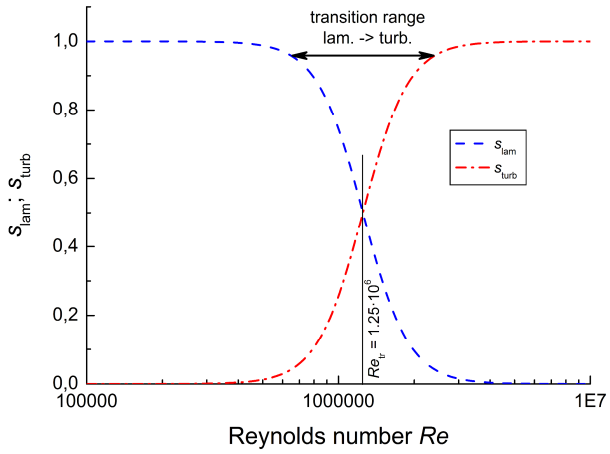

Figure 1: Weighing factors s_{lam} and s_{turb} to model the transition from laminar to turbulent boundary layers in dependency on Reynolds number Re.

All the relations given by Equations (4) to (9) and the pre-setting of k_u as well as Re_{tr} provide our base to adopt b_{lam} as the only free parameter and to get the overall functionality for the discharge coefficient from low to high Reynolds numbers.

2. Data evaluation

2.1 Data base

There are many information on calibration from the past years available in the data base of PTB. For the best proof of our approach in this paper, we choose all nozzles with the constrains that the highest Reynolds number shall be above $Re \geq 2.5 \cdot 10^6$ to reach the region of turbulent boundary layers based on our measurement capabilities. Consequently, the throat diameter shall be at least 3.8 mm. Finally, data of 33 nozzles have been chosen. Their main specifications are listed in Table 1.

All nozzles are in principle designed based on the ISO 9300. The diameters ranges from 3.8 mm to 46.6 mm and the design curvature radius (normalised with the throat diameter) is $R_{C,design} = 1$ for seven nozzles and $R_{C,design} = 2$ for 24 nozzles. One nozzle has $R_{C,design} = 2.5$ and one is a cylindrical nozzle.

In Table 1, there is the Reynolds number Re_0 given what is achieved for the nozzles when operated with air at 100 kPa. Additionally, we noted in Table 1 the minimum and maximum of expanded uncertainties of the flow rate measurements in the range of Reynolds numbers for $Re/Re_0 \geq 8$. This is the range where we have data gathered with natural gas based on the traceability of PTB for high pressure natural gas.

Beside the data with high pressure natural gas based on PTB traceability, there are some nozzles where also other data are available. Nozzles #15, #21 and #33 were used in inter comparison in the year 2015 and LNE-LADG as well as NIM provided data based on high pressure air. The data and related information are already published in [1]. Nozzle #32 was used in an inter comparison between NIST, LNE-LADG and PTB in 2005 [7]. Hence, for this we have additionally data with nitrogen and air. Finally, the nozzles #11, #19 and #26 have been calibrated with high pressure nitrogen on customer site [8].

The diameters of all nozzles listed in Table 1 have been measured by means of 3D-CMM at PTB, an accredited laboratory or one of the other partners in the inter comparisons mentioned above. We claim an expanded uncertainty of 3 µm for the diameter. This value is based on the comparison of repeated measurements of 9 sonic nozzles (with d_{throat} from 5 to 10 mm) with long time difference.

Table 1: Main information on data base.

Noz. Nr.	d_{throat} in mm	$R_{C,design}$	Re_0 (100 kPa, air)	for $Re/Re_0 \geq 8$; $k = 2$	
				$U_{Q,min,rel}$	$U_{Q,max,rel}$
1	7,098	1	9,20E4	0,07%	0,15%
2	10,780	1	1,40E5	0,16%	0,16%
3	15,250	1	1,98E5	0,16%	0,16%
4	21,320	1	2,76E5	0,16%	0,16%
5	26,950	1	3,49E5	0,16%	0,16%
6	34,280	1	4,45E5	0,16%	0,16%
7	46,560	1	6,04E5	0,16%	0,16%
8	3,808	2	4,94E4	0,07%	0,15%
9	3,893	2	5,05E4	0,15%	0,15%
10	3,897	2	5,05E4	0,19%	0,24%
11	3,903	2	5,06E4	0,15%	0,15%
12	4,331	2	5,62E4	0,19%	0,20%
13	4,344	2	5,63E4	0,19%	0,22%
14	4,938	2	6,40E4	0,12%	0,12%
15	4,945	2	6,41E4	0,08%	0,14%
16	5,486	2	7,11E4	0,19%	0,25%
17	5,492	2	7,12E4	0,18%	0,23%
18	6,142	2	7,96E4	0,08%	0,12%
19	6,657	2	8,63E4	0,15%	0,15%
20	6,987	2	9,06E4	0,17%	0,19%
21	6,988	2	9,06E4	0,08%	0,14%
22	7,027	2	9,11E4	0,07%	0,15%
23	7,453	2	9,66E4	0,07%	0,15%
24	7,768	2	1,01E5	0,08%	0,12%
25	9,911	2	1,29E5	0,12%	0,12%
26	11,258	2	1,46E5	0,15%	0,15%
27	12,293	2	1,59E5	0,16%	0,18%
28	15,478	2	2,01E5	0,10%	0,12%
29	19,376	2	2,51E5	0,10%	0,12%
30	24,551	2	3,18E5	0,10%	0,12%
31	31,253	2	4,05E5	0,12%	0,12%
32	25,400	2,5	3,29E5	0,18%	0,19%
33	10,000	cylindr.	1,30E5	0,07%	0,13%

2.2 Illustration of approach for two nozzles

In Figure 2 there are all the single measurement data shown for the nozzles #1 and #22 of Table 1. Both have similar diameter of about 7 mm but different design curvature radius: $R_{C,design} = 1$ for nozzle #1 and $R_{C,design} = 2$ for nozzle #22. The real local curvature radii are shown in Figure 3 based on the dimensional measurements with 3D-CMM.

For the determination of the parameter b_{lam}, only the values of discharge coefficients c_D measured at Reynolds numbers below $Re = 10^5$ were used. They are indicated with dark blue colour. All other data with air are shown in light blue and those with natural gas in red.

The first step is the calculation of the Likelihood-function for the measured c_D-values depending on the parameter b_{lam}. The base for this is the function of c_D depending on b_{lam} according Equation (5) and (7). The result for our two exemplary nozzles is shown in Figure 4 at the Reynolds number $Re = 9.1 \cdot 10^4$. The corresponding measured values $c_{D,measured}$ are shown as well. For each point at the

curve of $c_D(b_{lam}, Re = 9.1 \cdot 10^4)$ we get a distance to the $c_{D,meas}$ and taking the uncertainty of $c_{D,meas}$ into account we get the likelihood $L(c_{D,meas}|b_{lam})$ of this $c_{D,meas}$ if a specific b_{lam} is given.

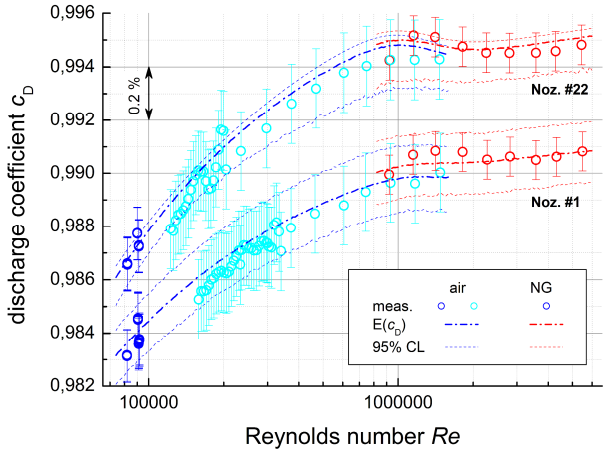

Figure 2: Exemplary date of two nozzles with the designed throat curvature radii $R_{C,design}$ = 1 (#1)and $R_{C,design}$ =2 (#22), see also Table 1.

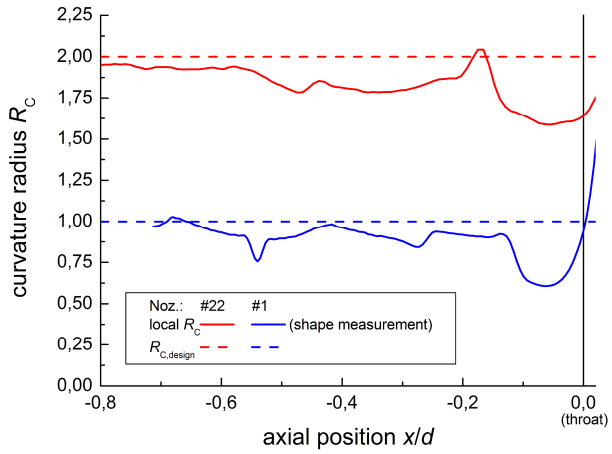

Figure 3: Local curvature radii R_C of the nozzles #1 and #22 in the inlet section upstream to the throat ($x/d \leq 0$) based on dimensional shape measurements.

In Figure 5, there are the final Likelihood functions given for nozzles #1 and #22. Please note that this is already the Likelihood for all data $c_{D,meas}$ with Re < 10^5 (see Figure 2).

As you can see in Figure 5, the outcome of the Likelihood function can be asymmetric and may have also a separated second peak (here for nozzle #1). This means that there would be also a second but totally different value for b_{lam} what would fit to the measured c_D-values. To exclude such ranges, we need to include further information in the sense of a prior probability $p_{prior}(b_{lam})$. We can apply the basic Bayesian formulation between Likelihood, prior and posterior as given in Equation (10):

$$p(b_{\mathrm{lam}}|c_{\mathrm{D,meas}}) \sim L(c_{\mathrm{D,meas}}|b_{\mathrm{lam}}) \cdot p_{\mathrm{prior}}(b_{\mathrm{lam}}) \quad (10)$$

In our case, we make only use of priors with $p_{prior}(b_{lam})$ = const. for all b_{lam} within $0 \leq b_{lam} \leq b_{lam,max}$. The $b_{lam,max}$ can be derived from the information about the design curvature radius $R_{C,design}$ or the local values of R_C out of shape measurements, e.g. $b_{lam,max} = 2.9 R_{C,max}^{0.25}$ with $R_{C,max} = 2 \cdot R_{C,design}$. E.g., in the case of nozzle #1 we get $b_{lam,max}$ = 3.5. With such prior we introduce of course restrictions to the quality of the nozzles shape so that overall the local shape curvature radius shall not be larger than two times of the designed value. Looking to Figure 3, this restriction seems reasonable and not very strong.

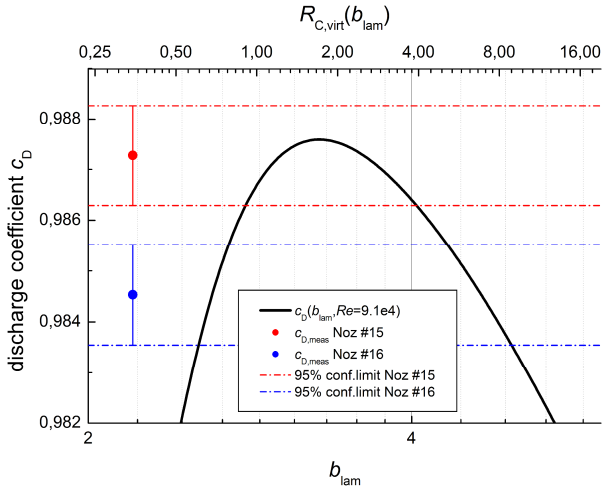

Figure 4: c_D as a function depending on b_{lam} for Re = 9.1·10^4 compared to the measured c_D-values for nozzle #1 and #22.

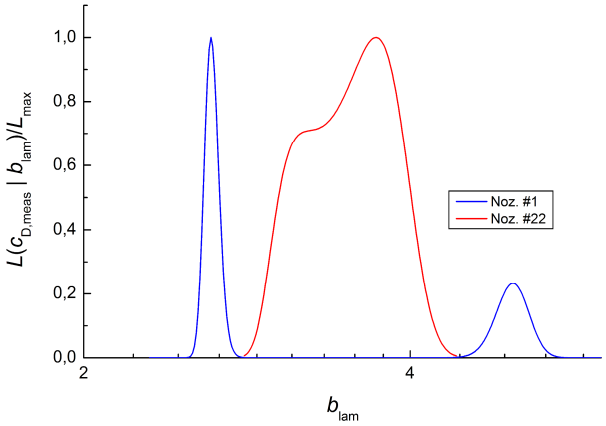

Figure 5: Likelihood of measured c_D-values for all data $Re \leq 10^5$ in Figure 2.

With the probability density $p(b_{lam}|c_{D,meas})$ we can determine in the next step the related probability density of (predicted) c_D-values for any other Reynolds number using a Monte Carlo approach. We generate (e.g.) 10.000 random numbers z_i equally distributed in the range [0,1) and transform these numbers using the inverse probability function $P^{-1}(b_{lam}|c_{D,meas})$ to get the set of random $b_{lam,i}$ with the probability density $p(b_{lam}|c_{D,meas})$. For all these $b_{lam,i}$ the $c_{D,expol,i}$ at the intended Reynolds number(s) are calculated. We use the expectation value $E(c_{D,extrapol,i})$ for the final predicted value. Looking to Figure 2, it can be obtained that the outcome for $c_{D,extrapol,i}$ can be significantly asymmetric (nozzle #22) and the 95%-confidence limits are asymmetric to the expectation value.

2.3 Results

The straight forward check of our approach is the comparison of the extrapolated $c_{D,extralpol}$ with all the data measured at pressures ≥ 110 kPa which were not used for the parameter determination. In Figure 6 we plotted the differences

$$\Delta_{c_D} = c_{D,meas} - c_{D,extrapol} \qquad (11)$$

versus the Reynolds number *Re*. The same data are shown in Figure 7 plotted versus the ratio of Reynolds numbers Re/Re_0 (for Re_0 see Table 1).

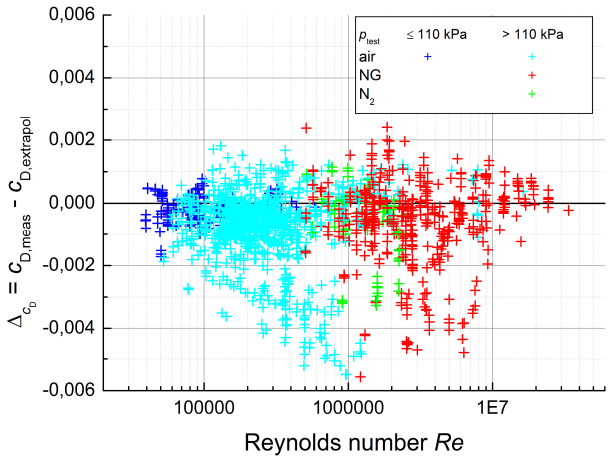

Figure 6: Differences Δ_{cD} of the measured discharge coefficients $c_{D,meas}$ to the extrapolated $c_{D,extrapol}$ in dependency on the Reynolds number.

The histogram in Figure 8 summarizes all data with $Re/Re_0 \geq 8$ for the evaluation of extrapolation because in this range the data origin mainly from the traceability for high pressure natural gas at PTB. This traceability is independent to the traceability for low pressure air.

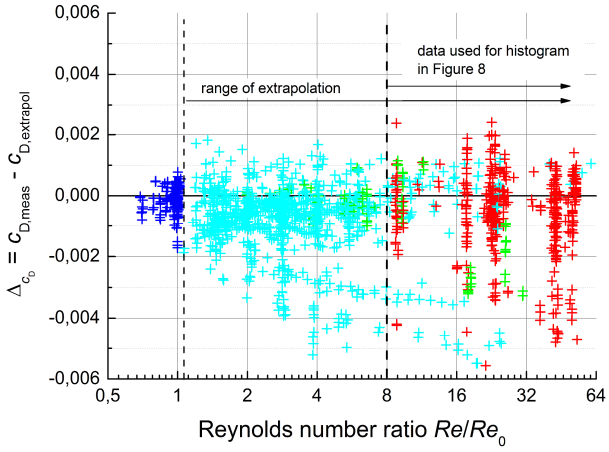

Figure 7: Differences Δ_{cD} of the measured discharge coefficients $c_{D,meas}$ to the extrapolated $c_{D,extrapol}$ in dependency on the ratio of Reynolds numbers Re/Re_0 (for Re_0 see Table 1).

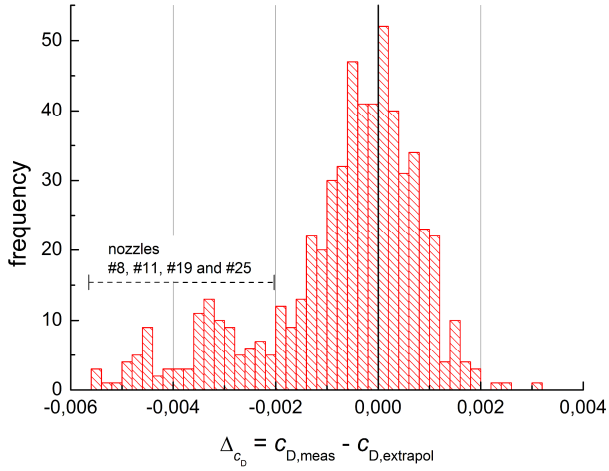

Figure 8: Histogram of differences Δ_{cD} for the ratio of Reynolds numbers $Re/Re_0 \geq 8$ (for Re_0 see Table 1).

The differences Δ_{cD} are almost within ±0.002, i.e. ±0.2 % of c_D. The values significantly outside of this limit can be allocated to four nozzles (#8, #11, #19 and #25) and are tending to negative deviations (means that the measured values are below the extrapolated).

The more detailed evaluation for each nozzle is using the value 0.002 as a normalisation factor for the single Δ_{cD}. All values belonging to one nozzle are summarised to a mean value $\Delta_{cD,mean}$ and are shown in Figure 9 and Figure 10. The error bars are the doubled standard deviation of the data set for each nozzle.

In Figure 9, the $\Delta_{cD,mean}$ are plotted versus the nominal diameter of the nozzles and it can be obtained that there is no significant tendency visible

except that the scatter seems to be little larger for the smaller diameters. As mentioned above, most of data exceeding the limit 0.002 can be assigned to the nozzles #8, #11, #19 and #25.

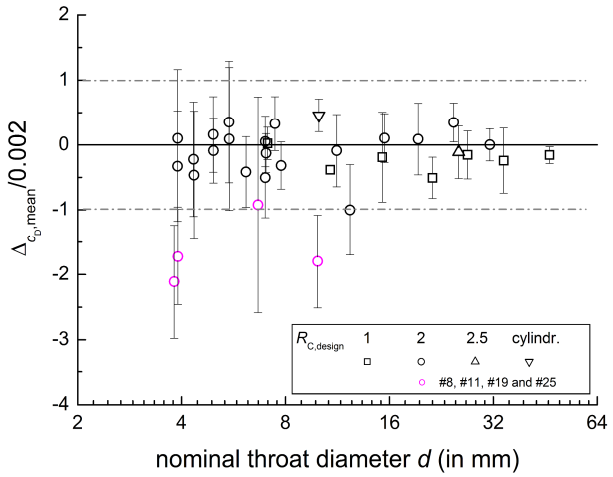

Figure 9: Histogram of normalised mean differences $\Delta_{cD,mean}$ for each nozzle and ratio of Reynolds numbers $Re/Re_0 \geq 8$ plotted versus the nominal diameter of the nozzles.

In Figure 10, same data as in Figure 9 are plotted versus the virtual curvature Radius $R_{C,virt}$ of the nozzles. Here, a slight tendency can be detected that the $\Delta_{cD,mean}$ are little lower for small $R_{C,virt}$ than for large $R_{C,virt}$. But this trend is not yet strong significant as the regression coefficient for a linear trend versus the log-scale of the diagram is 0.7 only.

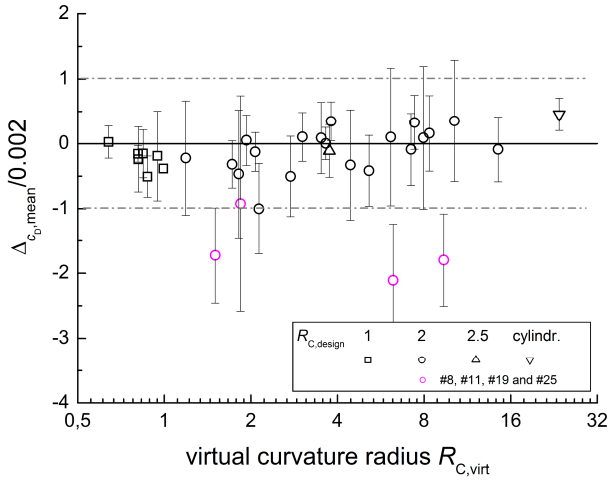

Figure 10: Histogram of normalised mean differences $\Delta_{cD,mean}$ for each nozzle and ratio of Reynolds numbers $Re/Re_0 \geq 8$ plotted versus the resulting virtual curvature Radius $R_{C,virt}$ of the nozzles.

In Table 2, some main results are summarized for all nozzles. Beside the virtual curvature radius $R_{C,virt}$ and the normalised mean differences $\Delta_{cD,mean}$, the minimal and maximal standard uncertainty of the extrapolated c_D-values in the range for $Re/Re_0 \geq 8$ are given. These standard uncertainties are within 0.02 %and 0.09 % except for the two nozzles #12 and #13. Please note that the probability density of the extrapolated c_D-values can be asymmetric so that a simple coverage factor cannot be applied in all cases to get the 95% coverage interval.

Table 2: Main results of the extrapolation.

Noz. Nr.	$R_{C,virt}$	$\Delta c_{D,mean}$ /0.002	for $Re/Re_0 \geq 8$; $k = 1$	
			$u_{extrapol,min}$	$u_{extrapol,max}$
1	0,64	0,02	0,06%	0,06%
2	0,99	-0,38	0,07%	0,08%
3	0,95	-0,19	0,06%	0,06%
4	0,87	-0,51	0,06%	0,06%
5	0,84	-0,15	0,06%	0,06%
6	0,81	-0,24	0,06%	0,06%
7	0,81	-0,16	0,06%	0,06%
8	6,24	-2,11	0,02%	0,04%
9	4,44	-0,33	0,02%	0,04%
10	6,13	0,10	0,02%	0,04%
11	1,50	-1,72	0,07%	0,08%
12	1,19	-0,22	0,14%	0,16%
13	1,81	-0,47	0,17%	0,21%
14	8,34	0,16	0,02%	0,05%
15	14,47	-0,09	0,02%	0,05%
16	10,20	0,35	0,02%	0,04%
17	7,96	0,09	0,02%	0,04%
18	5,15	-0,42	0,02%	0,04%
19	1,84	-0,92	0,04%	0,05%
20	2,75	-0,50	0,05%	0,07%
21	1,93	0,05	0,04%	0,06%
22	2,07	-0,13	0,04%	0,05%
23	7,41	0,33	0,02%	0,04%
24	1,72	-0,32	0,05%	0,06%
25	9,36	-1,80	0,03%	0,04%
26	7,20	-0,09	0,03%	0,04%
27	2,13	-1,00	0,02%	0,02%
28	3,02	0,11	0,05%	0,06%
29	3,51	0,09	0,06%	0,06%
30	3,80	0,35	0,06%	0,07%
31	3,64	0,00	0,05%	0,06%
32	3,75	-0,11	0,03%	0,04%
33	23,60	0,46	0,06%	0,09%

3. Discussion of the results

The main outcome of the results is that our extrapolation of c_D based on the measurements with low pressure air is in close agreement within 0.2% with the measured values even in the high Reynolds number range above $Re/Re_0 \geq 8$. Only the values of four out of 33 nozzles were detected as real outliers. Ignoring these outliers, there is no dependency of the agreement on the scale of extrapolation (Re/Re_0), see Figure 7.

The outliers can be explained at one hand with a very strong variance of the local curvature radius in the inlet of the nozzles. This e.g. the case for nozzles #19 what has a high peak in the curvature radius short before the throat (documented in [8]).

On the other hand, our approach to link the b_{lam} with b_{turb} via Equation (8) can be applied only for hydraulic smooth surfaces in the nozzles. In cases of significant roughness this relation will not apply what can be concluded from publication dealing with rough nozzles [9]. A significant roughness would also explain that the measured values for the outliers tend to be lower than the extrapolated values.

The data base contains a wide range of nozzles shapes with four different design curvature radii (see Table 1). The real shape of the nozzles close to the throat is even wider distributed what can be concluded from the resulting virtual curvature radius with values $0.64 \le R_{C,virt} \le 23.6$.

The approach of the extrapolation is based on the assumption that the virtual curvature Radius $R_{C,virt}$ is a constant all over the Reynolds number range investigated. This can be assumed for nozzles larger than a minimum size (i.e. above a minimum Reynolds number) but it is a simplification what will be not valid anymore for small nozzles (see for this e.g. [6]). Such additional dependency might be also the reason for the slight trend of the $\Delta_{cD,mean}$ versus the $R_{C,virt}$.

The mathematical model for the overall function of $c_D(Re)$ introduced above in section 1.2 contains the arbitrary values for k_u = 5.5 and Re_{tr} = $1.25 \cdot 10^6$. When looking to Figure 6, we can obtain that there is no significant enlargement of the Δ_{cD} in the range of $7 \cdot 10^5 \le Re \le 2.5 \cdot 10^6$, so that these values are again confirmed as reasonable empirical values to model the transition region using Equation (9) for a wide variety of nozzles.

The standard uncertainties of the measured c_D-values at high Reynolds numbers are typically in the order of 0.06 to 0.08 % (see Table 1, note that the table provides the expanded uncertainties with k = 2). This is the same level as we got for the extrapolated values (Table 2). The empirical limit of 0.2 % out of the histogram in Figure 8 (excluding the outliers and interpreted as a 95%-confidence level) is in good agreement with the combination of both the experimental and extrapolated uncertainty. Therefore, we can conclude that the uncertainty derived from the extrapolation process is reliable.

4. Conclusion

We presented a mathematical model for the functionality of the discharge coefficient c_D versus Reynolds number covering laminar and turbulent boundary layers as well. It contains only one free parameter b_{lam} what can be determined therefore using the c_D-values measured in a narrowed range of Reynolds numbers with atmospheric air.

The outcome of this fitted model has been used for wide ranged extrapolation up to a factor of 60 in the Reynolds number. It was compared against a large dataset of experimental c_D-values of 33 nozzles. The agreement between experimental and extrapolated values were almost within 0.2 % for 29 of the 33 nozzles what confirms the reliability of the model and the related extrapolation. This agreement is independent to the design curvature radius as well as the resulting virtual curvature radius and covers a wide range of nozzles shapes.

Therefore, we could demonstrate that it is possible to extrapolate low pressure calibrations of sonic nozzles to high pressure application range with a reasonable uncertainty so that we can use such sonic nozzles to underfeed our traceability for high pressure gas additionally with a link to our low-pressure traceability chain.

The approach can be extended in two directions. First, the parameter determination should be applied to experimental values out of a larger range of Reynolds numbers. The larger the Re-range the more precisely the parameters can be determined. With such extended Re-range for parameter fitting, we can introduce also the throat diameter as a free parameter in the mathematical model.

Second, it is promising to refine the Bayesian approach in Equation (10), specifically when we will adopt also the diameter to the experimental data. A more specific formulation of the prior knowledge about the curvature radius and its impact to the parameter b_{lam} as well as the throat diameter gathered by dimensional measurements will enhance the reliability of such extrapolation.

References

[1] Mickan, B., Vallet, J.-P., Li, C., Wright, J.: *Extended data analysis of bilateral comparisons with air and natural gas up to 5 MPa*, FLOMEKO 2016, Sydney, Australia, September 26-29, 2016

[2] Kliegel, J. R., Levine, J. N.: *Transonic Flow in Small Throat Radius of Curvature Nozzles*, AIAA Journal Vol 7, nr. 7, 1969, pp. 1375 - 1378

[3] Geropp, D., *Laminare Grenzschichten in ebenen und rotationssymmetrischen*

Lavalduessen, Deutsche Luft- und Raumfahrt, Forschungsbericht 71-90, 1971.

[4] Geropp, D., *Laminare Grenzschichten in Überschalldüsen*, Deutsche Luft- und Raumfahrt, Forschungsbericht 01 TM 8603-AK/PA 1, 1987.

[5] Wright, J. et al, *Thermal Effects on Critical Flow Venturis*, Proceedings of 9th International Symposium on Fluid Flow Measurement, Arlington, Virginia, 2015.

[6] Mickan, B. et al, *Systematic investigations of cylindrical nozzles acc. ISO 9300 down to throat diameters of 125 µm*, Proceedings of 10th International Symposium on Fluid Flow Measurement, Queretaro, Mexico, 2018.

[7] Mickan, B., Kramer R., Dopheide D., Hotze, H.-J., Hinze, H.-M., Johnson, A., Wright, J., Vallet, J.-P., *Comparisons by PTB, NIST, And LNE-LADG in Air and Natural Gas with Critical Venturi Nozzles agree within 0.05 %*, Proceedings of 6th International Symposium on Fluid Flow Measurement, Queretaro, Mexico, 2006.

[8] Mickan, B., Kramer, R., *Experiences With Sonic Nozzles Used For Different Gases And Wide Range Of Pressure And Temperature Conditions*, Proceedings of 7th International Symposium on Fluid Flow Measurement, Anchorage, Alaska, 2009.

[9] Lambert, M.-A. et al., *Numerical and Experimental Investigations on the Shape and Roughness of Cylindrical Critical Flow Venturi Nozzles (CFVN)*, Proceedings of 10th International Symposium on Fluid Flow Measurement, Queretaro, Mexico, 2018.